

# High Three-Dimensional Thermoelectric Performance from Low-Dimensional Bands

David Parker, Xin Chen, and David J. Singh

*Materials Science and Technology Division, Oak Ridge National Laboratory, 1 Bethel Valley Road, Oak Ridge, Tennessee 37831-6056, USA*

(Received 12 November 2012; published 2 April 2013)

Reduced dimensionality has long been regarded as an important strategy for increasing thermoelectric performance, for example, in superlattices and other engineered structures. Here we point out and illustrate by examples that three-dimensional *bulk* materials can be made to behave as if they were two dimensional from the point of view of thermoelectric performance. Implications for the discovery of new practical thermoelectrics are discussed.

DOI: [10.1103/PhysRevLett.110.146601](https://doi.org/10.1103/PhysRevLett.110.146601)

PACS numbers: 72.20.Pa, 71.15.Mb

*Introduction.*—Thermoelectric performance is quantified by the figure of merit,  $ZT = \sigma S^2 T / \kappa$ , where  $\sigma$  is the electrical conductivity,  $\kappa$  is the thermal conductivity,  $S$  is the thermopower (Seebeck coefficient), and  $T$  is the absolute temperature [1,2]. There is no known thermodynamic or other fundamental limitation on  $ZT$ , but finding high  $ZT$  materials is very challenging and only a few materials with  $ZT$  significantly higher than unity are known. The difficulty is that finding high  $ZT$  requires finding a material that combines transport properties that do not normally occur together. Here we focus on the combination of high thermopower and high conductivity.

The low  $T$  electrical conductivity of a metal or degenerate semiconductor depends on the electronic states and their scattering at the Fermi level  $E_F$ , specifically  $\sigma \propto N(E_F) \langle v^2 \rangle \tau$ , with  $N$  the density of states,  $\langle v^2 \rangle$  the average Fermi velocity for the current direction, and  $\tau$  an inverse scattering rate [3,4]. The conductivity therefore improves as one moves  $E_F$  away from the band edge, as in that case both the velocity and  $N(E_F)$  increase. The thermopower is different. At low  $T$ ,  $S(T) \propto T(d\sigma/dE)/\sigma$ ; i.e.,  $S/T$  is large near the band edge where the logarithmic derivative of  $\sigma$  with energy is high.

Hicks and Dresselhaus suggested overcoming this conundrum via quantum well structures [5]. They observed that in a two-dimensional system the dependence of  $N(E)$  on energy for a parabolic band is a step function, meaning that for the in-plane direction one expects a faster onset of the conductivity with energy and, furthermore, higher  $S$  for given carrier concentration. Viewed in three dimensions, the Fermi surfaces of superlattices or two-dimensional semiconductors are in the shape of cylinders or pipes running along the direction of the layering rather than the spheres or ellipsoids of three-dimensional doped semiconductors.

However, most thermoelectric applications involve macroscopic devices that are difficult to implement with superlattices and experience problems such as parasitic heat conduction in barrier layers of superlattices. Nonetheless,

one observes that  $\text{Na}_x\text{CoO}_2$ , representative of the highest performance oxide thermoelectrics and showing high  $ZT$  at high carrier concentration [6], has a very two-dimensional electronic structure [7]. This material illustrates another problem with using 2D electronic systems as thermoelectrics. The high electrical conductivity is realized only in the layers, not perpendicular to them, while the heat conduction is more isotropic. Very high  $ZT$  is therefore realized only in single crystals for in-plane conduction or at least in highly textured ceramic. Here we propose an alternate resolution of the conundrum of high  $\sigma$  and high  $S$  using low-dimensional electronic structures.

We observe that it is possible to have an electronic structure that is low dimensional in a material that is not low dimensional provided that symmetry is obeyed. This is known in metallic materials, the best example being body centered cubic Cr metal, where flat (i.e., 1D) parts of the Fermi surface yield a nesting induced spin density wave [8]. Another example is the superconductor  $\text{Sr}_2\text{RuO}_4$ , which despite its tetragonal symmetry has flat one-dimensional sheets of Fermi surface that generate nesting induced peaks in its susceptibility [9,10]. Generally, these cases are large Fermi surface metals, which are not of interest as thermoelectrics. However, there is no symmetry or other fundamental reason that this must be so, and we begin by pointing out counterexamples.

The face centered cubic rocksalt structure chalcogenides, PbTe, PbSe, PbS and SnTe, are the basis of excellent thermoelectric materials [1,2]. While the thermoelectric properties of these materials have been discussed in terms of various physical models, band structure calculations combined with standard Boltzmann transport theory can reproduce and predict their thermopowers, as illustrated by predictions for PbSe [11,12]. As is well known, the valence band ( $p$ -type) electronic structure is dominated by  $L$ -point hole pockets for low carrier concentrations and  $T$ , while at higher carrier concentrations and  $T$  transport and other data imply additional electronic features, often discussed as a second heavy band [13–15]. Band structure calculations show no second heavy band, but instead connections

developing between the  $L$ -point pockets near, but not at, the valence band maximum.

We illustrate this in Fig. 1, which shows energy isosurfaces for the near valence band edge of PbTe, PbSe, PbS and SnTe. These are based on calculations, including spin orbit, done with the augmented plane wave plus local orbital method [16], as implemented in the WIEN2K code [17]. We employed the modified Becke-Johnson potential of Tran and Blaha [18], which generally gives improved band gaps for simple semiconductors and insulators [18–20]. Besides these details, the calculations are similar to those presented previously [11,21–29]. The densities of states (not shown) show low values characteristic of a light band up to the energy where the  $L$ -point pockets connect, where there is a sharp onset of a steeply rising density of states, which is clearly beneficial for obtaining enhanced  $S(T)$  at doping levels near the onset and was discussed in relation to the thermoelectric performance of PbTe [26]. Here we associate this with the pipes.

Qualitatively, the Fermi surface of a doped superlattice or other 2D semiconductor is cylindrical running along the stacking direction. The conductivity is low along the cylinder and high in the plane. Considering, for example, the conductivity along  $x$  for a cubic network of pipes running along  $k_x$ ,  $k_y$ , and  $k_z$ , as is approximately the case in these materials, the pipes along  $k_y$  and  $k_z$  will contribute as in a superlattice material in plane, while the pipes along  $k_x$  will behave like the stacking direction and will not contribute to the conductivity. Thus the energy dependence and other behaviors are the same as the superlattice, including the enhanced 2D behavior of the thermopower, except that

now the properties are isotropic due to the cubic symmetry and superposition of pipes on different directions.

Clearly, the electronic structures of the chalcogenides shown in Fig. 1 are approximations of this idealized behavior. Nonetheless, they suggest elucidation of the behavior of a cubic or other three-dimensional semiconductor with a low-dimensional electronic structure in the sense discussed above. This may be a useful paradigm in the search for new high performance thermoelectric materials.

*Calculations.*—Here we pursue calculations to describe the behavior of the transport in the aforementioned “pipes” scenario. We consider a one band material with a pipelike electronic structure, beginning by assuming the electronic scattering time  $\tau(E)$  independent of energy, i.e., the constant scattering time approximation (CSTA). This has been used with quantitative accuracy to describe the thermopower of a substantial number of thermoelectric materials [26,30–37], so its usage is on solid practical grounds. We also present results for the thermopower and power factor in a case where  $\tau(E)$  is inversely proportional to the electronic density of states, as considered in Refs. [38–40]; we will see that this model (which we term DSTA) renders the two-dimensional electronic structure scenario even *more* favorable relative to the three-dimensional electronic structure scenario. Note also that here we consider two-dimensional *electronic* structures in *bulk* materials as opposed to the two-dimensional *physical* structures in *nonbulk* materials [41] such as nanowires, considered in Refs. [39–41].

Then we have the canonical expressions for the electrical conductivity  $\sigma(T)$  and Seebeck coefficient  $S(T)$ :

$$\sigma(E) = N(E)v^2(E)\tau(E), \quad (1)$$

$$\sigma(T) = - \int_{-\infty}^{\infty} dE \sigma(E) df(E - \mu)/dE, \quad (2)$$

$$S(T) = - \frac{k_B}{e\sigma(T)} \int_{-\infty}^{\infty} dE \sigma(E) \frac{E - \mu}{T} df(E - \mu)/dE, \quad (3)$$

with  $f$  the Fermi function,  $e$  the electronic charge,  $k_B$  Boltzmann’s constant,  $\tau(E)$  the scattering time,  $v(E)$  the Fermi velocity,  $\mu$  the chemical potential, and  $N(E)$  the density of states. The tensor indices are suppressed for clarity, and the integrations in actual calculations involve a Brillouin zone sum.

We now compare the thermopower and power factor  $S^2\sigma$  of two idealized Fermi surface topologies: a two-dimensional cylindrical Fermi surface connecting the  $L$  points of the fcc Brillouin zone, as suggested by Fig. 1, and a three-dimensional spherical Fermi surface. Note that in actual materials Fermi surfaces which contact Brillouin zone faces must do so at perpendicular angles, so the pipes reconnect at the  $L$ -point pockets, as in, for example, band structure calculations for PbTe. Both bands are assumed parabolic, and to ensure a fair comparison we choose the radial masses of the cylinder and sphere equal.

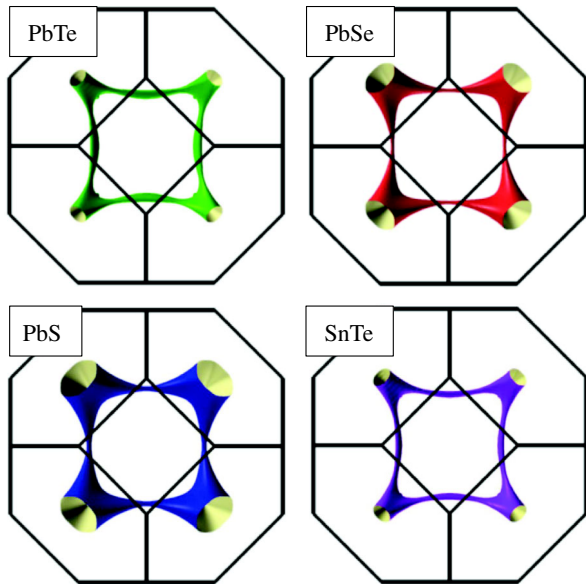


FIG. 1 (color online). Calculated valence band constant energy isosurfaces of PbTe, PbSe, PbS, and SnTe at 0.23, 0.49, 0.61, and 0.41 eV below the valence band maximum, respectively. The corresponding carrier concentrations in holes per unit cell are 0.016, 0.030, 0.054, and 0.016, respectively.

Additionally, as was noted by Ref. [42], in the chalcogenides the cylindrical band is 12-fold degenerate and we have assumed this here. For comparison purposes we take the spherical Fermi surface to be 12-fold degenerate.

Then within the CSTA the above integrals are easily evaluated for both cases, yielding the following expressions (here  $\eta = \mu/T$ , the reduced chemical potential):

$$S_{3D}(T) = \frac{5}{3} \frac{F_{3/2}(\eta)}{F_{1/2}(\eta)} - \eta, \quad (4)$$

$$\sigma_{3D}(T) = \frac{pe^2\tau}{m^*}, \quad (5)$$

$$S_{2D}(T) = 2 \frac{F_1(\eta)}{F_0(\eta)} - \eta, \quad (6)$$

$$\sigma_{2D}(T) = \frac{2pe^2\tau}{3m^*}. \quad (7)$$

Here  $p$  is the carrier density given as

$$p = \int dE N(E) f(E - \mu), \quad (8)$$

where  $N(E)$  is the density of states,  $m^*$  the carrier effective mass, and  $F$  is the Fermi-Dirac integral, defined as

$$F_i(\eta) = \int_0^\infty x^i / [\exp(x - \eta) + 1]. \quad (9)$$

The  $2/3$  factor for the two-dimensional conductivity arises because each of the cylinders contributing to  $N(E)$ , and hence  $p$ , conducts in only two of three directions. Finally, we incorporate the relation of the reduced chemical potential  $\eta$  to the carrier concentration  $p$ , which is performed by inverting Eq. (8), as in Ref. [43].

We now move to the calculated results. We have assumed (although the results do not sensitively depend on these assumptions) a fcc cell of lattice constant  $6.46 \text{ \AA}$ , band masses of  $0.2m_0$ , where  $m_0$  is the free electron mass, and fixed the temperature at  $1000 \text{ K}$ , the approximate maximum operating temperature of the chalcogenides. We assume a doping independent scattering time  $\tau$  of  $10^{-15} \text{ sec}$ , which yields high temperature conductivities of  $100\text{--}1000 (\Omega \text{ cm})^{-1}$ , in line with experimental results. Figure 2 depicts the calculated thermopower results for the two scenarios. The 2D thermopower exceeds the 3D values by a substantial margin throughout the entire range of  $0.001\text{--}0.5$  holes per unit cell. At the heavy dopings of  $0.05\text{--}0.1$  per unit cell, the 2D thermopower is nearly double the 3D value, which is highly favorable for thermoelectric performance, and this thermopower increase comes at a conductivity reduction [Eqs. (5) and (7)], relative to the 3D case, of only one-third.

The 2D power factor (Fig. 3) exceeds the 3D value across the entire range of concentration, and its maximum value is two and a half times the corresponding 3D maximum. It is highly likely that 2D performance (i.e.,  $ZT$ )

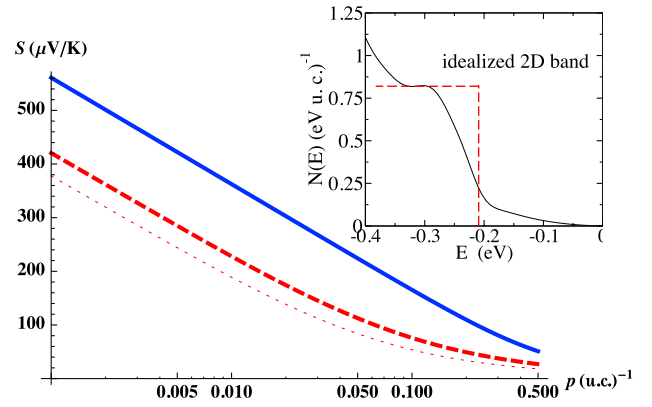


FIG. 2 (color online). (Main panel) The calculated thermopower for the 2D (blue solid line) and 3D (red dashed and dotted lines) cases. For the 2D case the CSTA and DSTA give identical results, while for the 3D case the CSTA results are the heavy dashed line and the DSTA results the dotted line. Carrier concentrations given per unit cell (u.c.). Inset: The first-principles calculated density of states of the two-dimensional electronic feature in PbTe, as depicted in Fig. 1.

would substantially exceed that of the 3D case. In the inset of Fig. 2 we depict a “real-world” example of this two-dimensional feature—the first-principles calculated valence band density of states of PbTe, the highest performance thermoelectric known [44]. The plot shows a feature very similar to a broadened step function expected for a two-dimensional feature. We emphasize that the notation 2D and 3D is to distinguish the cases, but that in both cases we are referring to the bulk, macroscopic measurable values for the cubic crystal.

Figure 2 also depicts the thermopower results within the DSTA. For the 2D case the DSTA is identical to the CSTA since the 2D density of states is constant with energy. For the 3D case, however, use of the DSTA results in a significant *decrease* in thermopower, as it preferentially weights the carriers nearest in energy to the band edge, where the DOS is lower and  $\tau(E)$  therefore larger. The upshot of this discussion is that, for the CSTA, the beneficial effect of two-dimensional electronic structures

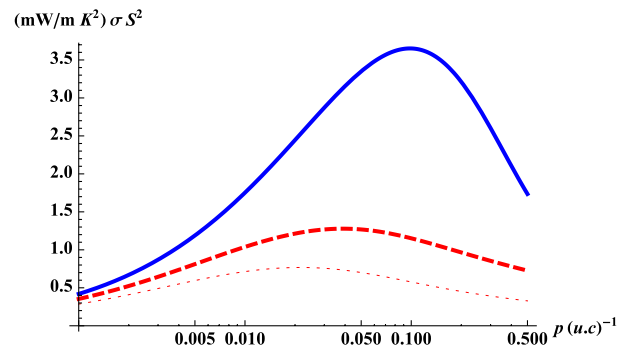


FIG. 3 (color online). The calculated power factor  $S^2\sigma$  in  $\text{mW/m K}^2$  for the 2D (blue solid line) and 3D (red dashed and dotted lines) cases. Same line conventions as in Fig. 2.

relative to three-dimensional ones is substantial, and that moving to the less-used DSTA only *increases* this effect.

*Analysis of enhanced Seebeck coefficient in the 2D case.*—The results of the previous section strongly suggest that the two-dimensional “pipe” topology is favorable for thermoelectric performance, particularly for the Seebeck coefficient, an indispensable ingredient of good thermoelectric performance. Here we provide analytic understanding of this result.

The enhanced behavior of the 2D system modeled here arises from the relatively larger Fermi surface volume (or, equivalently, carrier concentration) of a 2D cylinder relative to a 3D sphere, for given Fermi energy. The Fermi surface volume of the cylinder is proportional to the length of the cylinder  $= \frac{2\pi}{a}$ , a value much larger than the radius of the cylinder or the sphere, so that for given Fermi energy the carrier concentration is much larger. The Fermi energy is relevant because of the well-known Mott formula for the thermopower,

$$S = \frac{\pi^2 k_B}{3e} k_B T d \log[\sigma(E)] / dE|_{E=E_F}, \quad (10)$$

and for a parabolic 3D band yields

$$S = \frac{\pi^2 k_B}{2e} k_B T / E_F, \quad (11)$$

so the thermopower is inversely proportional to  $E_F$ . In two dimensions, at fixed carrier concentration  $E_F$  is much smaller than in three dimensions, and the thermopower is enhanced as a result.

To gain additional insight into this phenomenon and explore the effect of changing parameters, we perform analytic calculations within two well-known limits for which closed form results are available: the degenerate limit, when  $\eta \equiv E_F/T \gg 1$ , and the nondegenerate limit, when  $\eta < 0$ . Together these regimes account for most of the behavior of the thermopower in Fig. 1. We begin with the degenerate limit. In two dimensions, for radial mass  $m^*$ , it is easy to show (assuming a band degeneracy of 24, 2 for spin and 12 for the 12 pipes) that the thermopower takes the form

$$S_{2D} = \frac{\pi^2}{3} \frac{k_B}{e} \frac{3m^* a^2 k_B}{\pi \hbar^2 p}, \quad (12)$$

where  $p$  is the carrier concentration per unit cell, and similarly for 3D,

$$S_{3D} = \frac{\pi^2}{2} \frac{k_B}{e} \frac{2m^* a^2 k_B T}{\hbar^2 (\pi^2 p)^{2/3}}, \quad (13)$$

so that one finds that

$$S_{2D}/S_{3D} = (\pi/p)^{1/3}. \quad (14)$$

Since  $p$  is typically much less than unity,  $S_{2D}$  is substantially larger than  $S_{3D}$ . Numerically, for  $p = 0.5$  per unit cell (yielding an  $\eta_{2D}$  of 5.5), this ratio is 1.845, while the exact result is 1.747, a 6% difference.

We now treat the nondegenerate limit, which is specified by  $\eta \ll 0$ , so  $f(E - \mu)$  reduces to  $\exp\frac{\mu-E}{T}$  and the energy integrals can be done exactly. As is well known [45], the 3D parabolic band thermopower is given by

$$S(p, T)_{3D} = \frac{k_B}{e} \left[ \frac{5}{2} - \eta_{3D}(p, T) \right]. \quad (15)$$

For our 2D cylindrical parabolic band, one finds that

$$S(p, T)_{2D} = \frac{k_B}{e} [2 - \eta_{2D}(p, T)]. \quad (16)$$

Note that  $\eta_{2D}$  and  $\eta_{3D}$  vary due to the topology difference, and we now work out an expression for their difference. For two dimensions, the relation of  $\eta$  and  $p$  can be evaluated exactly and is simply

$$\eta_{2D} = \log \left[ \exp \left( \frac{\pi p}{3m^* T a^2} \right) - 1 \right], \quad (17)$$

and in the nondegenerate limit this becomes

$$\eta_{2D} = \log \left( \frac{\pi p}{3m^* T a^2} \right). \quad (18)$$

One can similarly work out an expression for  $\eta_{3D}$  in the nondegenerate limit, and one finds

$$\eta_{3D} = \log \left( \frac{4\pi^{3/2} p}{3(2m^*)^{3/2} a^3 T^{3/2}} \right), \quad (19)$$

so that, restoring the appropriate powers of  $\hbar$  and  $k_B$ , one finds that

$$\eta_{2D} - \eta_{3D} = -\log \left( \frac{m^{*1/2} a (k_B T)^{1/2}}{\sqrt{2\pi\hbar}} \right). \quad (20)$$

For the modeled situation ( $m^* = 0.2m_0$ ,  $T = 1000$  K,  $a = 6.46$  Å), the difference is  $-2.097$  so that in the nondegenerate limit one finds  $S_{2D} - S_{3D} = 1.597 k_B/e = 137$   $\mu\text{V/K}$ , which is very close to the difference in these values at the left-hand of Fig. 2. This is a substantial increase.

The last equation reveals that if the effective mass (which was chosen on the basis of effective masses in the chalcogenides and  $\text{Bi}_2\text{Te}_3$ ) is larger, the effective benefit in the nondegenerate limit is smaller, but for large effective mass materials one is typically closer to the degenerate limit. Conversely, if the temperature is smaller (such as for room temperature applications), the difference is correspondingly greater, provided the sample remains in the nondegenerate limit.

*Summary and Conclusions.*—To summarize, we have shown here that (1) low-dimensional electronic structures can occur even in cubic semiconductors and that (2) such electronic structures are highly beneficial for thermoelectric performance. This represents a new paradigm for high thermoelectric performance: low-dimensional electronic structures enhancing performance in fully three-dimensional bulk thermoelectrics. Examples of existing

materials in which this effect appears to be active are the high performance thermoelectrics PbTe, PbSe, and PbS. We suggest searching for new thermoelectric materials with this feature. One such compound may be SnTe [46,47].

This research was supported by the U.S. Department of Energy, EERE, Vehicle Technologies, Propulsion Materials Program (DP), the Solid State Solar-Thermal Energy Conversion Center (S3 TEC), an Energy Frontier Research Center funded by the U.S. Department of Energy, Office of Science, Office of Basic Energy Sciences under Award No. DE-SC0001299/DE-FG02-09ER46577 (X. C., D. J. S.).

- 
- [1] A. F. Ioffe, *Semiconductor Thermoelements and Thermoelectric Cooling* (Inforesarch, London, 1957).
- [2] C. Wood, *Rep. Prog. Phys.* **51**, 459 (1988).
- [3] J. M. Ziman, *Electrons and Phonons* (Oxford University Press, New York, 2001).
- [4] W. Jones and N. H. March, *Theoretical Solid State Physics* (Courier Dover Publications, 1985).
- [5] L. D. Hicks and M. S. Dresselhaus, *Phys. Rev. B* **47**, 16631 (1993).
- [6] I. Terasaki, Y. Sasago, and K. Uchinokura, *Phys. Rev. B* **56**, R12685 (1997).
- [7] D. J. Singh, *Phys. Rev. B* **61**, 13 397 (2000).
- [8] E. Fawcett, *Rev. Mod. Phys.* **60**, 209 (1988).
- [9] I. I. Mazin and D. J. Singh, *Phys. Rev. Lett.* **82**, 4324 (1999).
- [10] Y. Sidis, M. Braden, P. Bourges, B. Hennion, S. NishiZaki, Y. Maeno, and Y. Mori, *Phys. Rev. Lett.* **83**, 3320 (1999).
- [11] D. Parker and D. J. Singh, *Phys. Rev. B* **82**, 035204 (2010).
- [12] Q. Zhang, F. Cao, W. Liu, K. Lukas, B. Yu, S. Chen, C. Opeil, D. Broido, G. Chen, and Z. Ren, *J. Am. Chem. Soc.* **134**, 10031 (2012).
- [13] Y. I. Ravich, B. A. Efimova, and V. I. Tamarchenko, *Phys. Status Solidi B* **43**, 11 (1971).
- [14] Y. I. Ravich, B. A. Efimova, and V. I. Tamarchenko, *Phys. Status Solidi B* **43**, 453 (1971).
- [15] C. E. Ekuma, D. J. Singh, J. Moreno, and M. Jarrell, *Phys. Rev. B* **85**, 085205 (2012).
- [16] E. Sjostedt, L. Nordstrom, and D. J. Singh, *Solid State Commun.* **114**, 15 (2000).
- [17] P. Blaha, K. Schwarz, G. K. H. Madsen, D. Kvasnicka, and J. Luitz, *WIEN2k, An Augmented Plane Wave + Local Orbitals Program for Calculating Crystal Properties*, edited by Karlheinz Schwarz (Technische Universität Wien, Austria, 2001).
- [18] F. Tran and P. Blaha, *Phys. Rev. Lett.* **102**, 226401 (2009).
- [19] D. J. Singh, *Phys. Rev. B* **82**, 205102 (2010).
- [20] D. Koller, F. Tran, and P. Blaha, *Phys. Rev. B* **83**, 195314 (2011).
- [21] P. J. Lin and L. Kleinman, *Phys. Rev.* **142**, 478 (1966).
- [22] S. H. Wei and A. Zunger, *Phys. Rev. B* **55**, 13 605 (1997).
- [23] D. I. Bilec, S. D. Mahanti, and M. G. Kanatzidis, *Phys. Rev. B* **74**, 125202 (2006).
- [24] K. Hummer, A. Gruneis, and G. Kresse, *Phys. Rev. B* **75**, 195211 (2007).
- [25] L. Zhang, A. Grystiv, P. Rogl, E. Bauer, and M. Zehetbauer, *J. Phys. D* **42**, 225405 (2009).
- [26] D. J. Singh, *Phys. Rev. B* **81**, 195217 (2010).
- [27] L. Q. Xu, Y. P. Zheng, and J. C. Zheng, *Phys. Rev. B* **82**, 195102 (2010).
- [28] A. Svane, N. E. Christensen, M. Cardona, A. N. Chantis, M. van Schilfgaard, and T. Kotani, *Phys. Rev. B* **81**, 245120 (2010).
- [29] D. J. Singh, *Funct. Mater. Lett.* **03**, 223 (2010).
- [30] G. K. H. Madsen, K. Schwarz, P. Blaha, and D. J. Singh, *Phys. Rev. B* **68**, 125212 (2003).
- [31] L. Zhang, M.-H. Du, and D. J. Singh, *Phys. Rev. B* **81**, 075117 (2010).
- [32] K. P. Ong, D. J. Singh, and P. Wu, *Phys. Rev. B* **83**, 115110 (2011).
- [33] D. J. Singh and I. I. Mazin, *Phys. Rev. B* **56**, R1650 (1997).
- [34] T. J. Scheidemantel, C. Ambrosch-Draxl, T. Thonhauser, J. V. Badding, and J. O. Sofo, *Phys. Rev. B* **68**, 125210 (2003).
- [35] L. Bertini and C. Gatti, *J. Chem. Phys.* **121**, 8983 (2004).
- [36] L. Lykke, B. B. Iversen, and G. K. H. Madsen, *Phys. Rev. B* **73**, 195121 (2006).
- [37] Y. Wang, X. Chen, T. Cui, Y. Niu, Y. Wang, M. Wang, Y. Ma, and G. Zou, *Phys. Rev. B* **76**, 155127 (2007).
- [38] R. Kim, S. Datta, and M. S. Lundstrom, *J. Appl. Phys.* **105**, 034506 (2009).
- [39] J. E. Cornett and O. Rabin, *Appl. Phys. Lett.* **100**, 242106 (2012).
- [40] N. Neophytou and H. Kosina, *Phys. Rev. B* **83**, 245305 (2011).
- [41] N. Neophytou and H. Kosina, *J. Electron. Mater.* **41**, 1305 (2012).
- [42] Y. Pei, X. Shi, A. LaLonde, H. Wang, L. Chen, and G. J. Snyder, *Nature (London)* **473**, 66 (2011).
- [43] J. S. Blakemore, *Solid State Electron.* **25**, 1067 (1982).
- [44] K. Biswas, J. He, I. D. Blum, C.-I. Wu, T. P. Hogan, D. N. Seidman, V. P. Dravid, and M. G. Kanatzidis, *Nature (London)* **489**, 414 (2012).
- [45] G. S. Nolas, J. Sharp, and H. J. Goldsmid, *Thermoelectrics: Basic Principles and New Materials Developments* (Springer, Berlin, 2001).
- [46] P. B. Littlewood, B. Mihaila, R. K. Schulze, D. J. Safarik, J. E. Gubernatis, A. Bostwick, E. Rotenberg, C. P. Opeil, T. Durakiewicz, J. L. Smith, and J. C. Lashley, *Phys. Rev. Lett.* **105**, 086404 (2010).
- [47] Y. Tanaka, Z. Ren, T. Sato, K. Nakayama, S. Souma, T. Takahashi, K. Segawa, and Y. Ando, *Nat. Phys.* **8**, 800 (2012).
- [48] D. J. Singh and L. Nordstrom, *Planewaves Pseudopotentials and the LAPW Method* (Springer, Berlin, 2006), 2nd ed.